Oxygen carrier derived from ferric sludge for chemical looping combustion of MSW syngas: Waste derived material performance and carbon footprint assessment

Chat How Joewin Koh Yang[a,b,d], Guicai Liu[a,*], Wei Ping Chan[a], Ya Zhao[a], Mei Ping Vernette Chin[a], Wen Liu[a,c], Teik Thye Lim[a,d], Grzegorz Lisak[a,d,*]

[a] *Residues and Resource Reclamation Centre, Nanyang Environment and Water Research Institute, Nanyang Technological University, Singapore 637141, Singapore*
[b] *Interdisciplinary Graduate Program, Nanyang Technological University, 1 Cleantech Loop, Cleantech One, Singapore 637141, Singapore*
[c] *School of Chemistry, Chemical Engineering and Biotechnology, Nanyang Technological University, Singapore 637459, Singapore*
[d] *School of Civil and Environmental Engineering, Nanyang Technological University, Singapore 639798, Singapore*
[*] Corresponding authors at: Residues and Resource Reclamation Centre, Nanyang Environment and Water Research Institute, Nanyang Technological University, 1 Cleantech Loop, Clean Tech One, 637141, Singapore.
Email Address: g.lisak@ntu.edu.sg (G. Lisak), garner.liu@ntu.edu.sg (G. Liu)

Highlights

- Ferric sludge is an effective dual functioning waste-derived oxygen carrier (OC)
- Ferric sludge achieves > 88% combustion efficiency and > 71% HCl removal efficiency
- Stability of ferric sludge OC improved with the application of Al_2O_3 as support
- Ferric sludge is superior to iron ore for chemical looping combustion
- Carbon footprint of ferric sludge is lower than iron ore by 108.0 $kgCO_2/t$

Keywords: Water treatment sludge; Chemical looping combustion; Oxygen carrier; MSW syngas; HCl removal; Climate change impacts; Carbon footprint assessment

Abstract

The utilization of water treatment sludge (i.e., ferric sludge) was explored as the oxygen carrier (OC) for chemical looping combustion (CLC) of municipal solid waste (MSW) syngas. The performance of ferric sludge (FS) in CLC and simultaneous HCl removal was evaluated in a bench-scale fluidized bed, and was compared with iron ore (IO) as a benchmarked OC. The results show that FS (92%) performed better than IO (82%) in terms of syngas combustion efficiency and FS was able to remove HCl (77% removal efficiency) while IO was unable to remove any HCl. Comparison of reaction temperature reveals that FS performed better at lower CLC temperature between 800 °C and 850 °C. Agglomeration was observed when FS was used in extended CLC cycles. Thus, investigation of using inert α-Al_2O_3 support together with FS for extended CLC cycles was investigated. Agglomeration and sintering were drastically reduced and good combustion efficiency of 88% for H_2 and 74% for CO was attained. Carbon

footprint assessment illustrated that FS was superior as a greener material based on global warming potential of 20 and 100 years. Conversion of FS as an OC were characterized with 104.23 and 108.0 kgCO_2/t lower than IO for GWP-20 and GWP-100, exhibiting the competitiveness in the usage of waste-derived material in CLC. Hence, FS can be considered as a novel, cost-effective, and greener OC for CLC. The co-utilization of waste-derived material and waste-derived syngas through CLC would be an integrated solution for improved circularity and sustainability.

1 Introduction

Chemical looping combustion (CLC) has garnered great attention owing to its capability to concurrently harvest energy from fuel and produce an almost pure stream of CO_2 at its output, and is thus lauded as a potentially competitive CO_2 capture technology [1]. In CLC, fuel combustion is comprised of two separated reactions, coupled by the transportation of the oxygen carrier (OC) between an air reactor (AR) and a fuel reactor (FR) [2]. In the FR, the OC is reduced by a fuel source and subsequently transported into the AR where the OC is oxidized and regenerated by air. The OC is then circulated back to the FR to close the loop. For practical applications, the OC should be able to maintain its chemical reactivity and physical integrity during multiple cycles while also being widely available, easy to produce, low cost, and environmentally friendly [3]. In general, the active components in OCs are oxides of transitional metals (e.g Fe, Ni, Cu, Co, Mn, etc.). Therefore, many natural minerals and inorganic industrial solid waste rich in these metals are potential OC candidates for CLC process. Due to the low cost of these materials compared to synthetic OCs, these materials have garnered high interest in CLC research. The application of low-cost OCs may substantially reduce the CLC operation costs, making it more attractive as a potential CO_2 capture technology [4].

The low-cost OCs explored in literature include natural ores such as iron ore [5], copper ore [6], and manganese ore [7] and waste materials such as ash residues [3], copper slag [8], sewage sludge ash [9], furnace dust [10], and bauxite waste [11], all of which contained a critical content of transitional metal oxides [12]. For example, incineration bottom ash as OC utilizes Fe_2O_3 and $CaSO_4$ as its active components and achieved a high combustion efficiency of H_2 at 94.6% and CO at 80.2% [3]. OC derived from sewage sludge ash also utilizes Fe_2O_3 as the active component and was proven that it was able to undergo 20 CLC cycles using H_2 as the fuel in a thermogravimetric analyzer [9]. Separately, high combustion efficiency of syngas

between 84% and 89% was observed when using copper slag as OC with CuO, Fe_2O_3, and $CuFe_2O_4$ as the active components [8]. Therefore, water treatment sludge (WTS), specifically the ferric sludge with its rich ferric content (~42% wt% Fe), is one of the promising yet unexplored waste-derived OCs.

For WTS, the type of coagulant used in the water treatment process determines the type of sludge produced [13], whereby usage of ferric salts and alum salts produces ferric sludge and alum sludge respectively [14]. It is estimated that the amount of WTS produced worldwide is about 1 to 3% volume of raw water treated in the plants [15]. Yet, there is a statistical obscurity with regards to WTS production and disposal at an international level as statistics for both WTS and sewage sludge are usually combined into one category. It is known that WTS is commonly sent directly to landfills. This, however, is not a sustainable solution because land itself is a finite and valuable resource, thus landfilling practices will eventually incur high financial and environmental costs [16]. Given the potential of WTS as a valuable resource, there is a need to explore viable options to reuse sludge and reduce the future environmental and financial burden from landfilling it.

In WTS, other than Fe, the main components include various compounds containing primarily Ca, Al, Si and Na [17], which may be beneficial to the reactivity of an OC. Ca can improve the reactivity of iron-based OCs and alleviate the sintering of iron oxide during CLC [18]. Besides this, Ca can also remove HCl during CLC [19], with previous studies demonstrating that coating iron oxide with Ca can simultaneously remove HCl while ensuring good combustion efficiency [20]. Separately, aluminum oxides can act as a support for OCs to improve their mechanical property and stability by preventing contact of active sites between OCs [21]. Lastly, $CaSO_4$ can improve the performance of the OCs by influencing oxygen transport through $CaSO_4$-CaS conversion in chemical looping process [22]. Nevertheless, potential side reaction of $CaSO_4$ can generate H_2S in the flue gas, which will be a challenging issue [23].

Municipal solid waste (MSW) syngas contains acidic impurities such as HCl. Presence of chlorine in MSW can cause boiler corrosion [24] and dioxin generation [25]. OC derived from ferric sludge could possibly mitigate these adverse effects. Therefore, ferric sludge has the potential to be a novel and highly reactive waste-derived OC for CLC application of municipal solid waste (MSW) syngas. Overall, the co-utilization of waste material and waste-derived syngas through CLC could be a potential solution for renewable energy generation and resource

management.

This study aims to evaluate the feasibility of ferric sludge as an OC for CLC of MSW syngas. Its performance in CLC, simultaneous HCl removal, and regenerability were evaluated in a bench-scale fluidized bed reactor, using iron ore (IO) as a benchmark of low-cost OC. The evolution of the OC during CLC was investigated by comparing the OCs before and after CLC using XRD, FESEM, ICP-OES and BET. Potential issues with using ferric sludge in extended redox cycles were identified using ICP-OES and FESEM. α-Al_2O_3 was added as a support to mitigate these issues and was investigated by observing the performance of the OC under extended redox cycles examined in the fluidized bed. Lastly, carbon footprint assessment was applied to further determine the sustainability of using ferric sludge as a promising waste-derived OC.

2 Materials and methods

2.1 Preparation of OCs

Ferric sludge was obtained from a freshwater treatment facility (or commonly known as a waterworks) in Singapore, where ferric salt ($FeCl_3$) was used as a coagulant for water treatment. The dewatered sludge was collected and stored in the cold room at 7 °C before use. To prepare ferric sludge as an OC, it was calcined in air using a chamber furnace at 950 °C (heating rate of 15.5 °C/min) for 5 h. After calcination, the ferric sludge was further crushed, pelletized and sieved to obtain a size range of 0.25mm to 0.5mm. Commercial iron ore (hematite, imported by SG Labware) was applied as a natural mineral and was used as a benchmark against FS for a comparative study. The iron ore was sieved to obtain a size range of 0.063mm to 0.25mm and then calcined at 950 °C (heating rate of 15.5 °C/min) for 5 h. The prepared ferric sludge and iron ore will be denoted as FS and IO respectively.

2.2 Reactivity tests

To determine the redox performance of the OCs, a bench scale fluidized bed reactor was used as illustrated in Fig. 1. The reactor was a quartz tube with the inner diameter of 11 mm and was heated to 800~900 °C by an electrical furnace during operation. To conduct the reactions in CLC, the cyclic reduction and oxidation of OCs was conducted by switching the input gases.

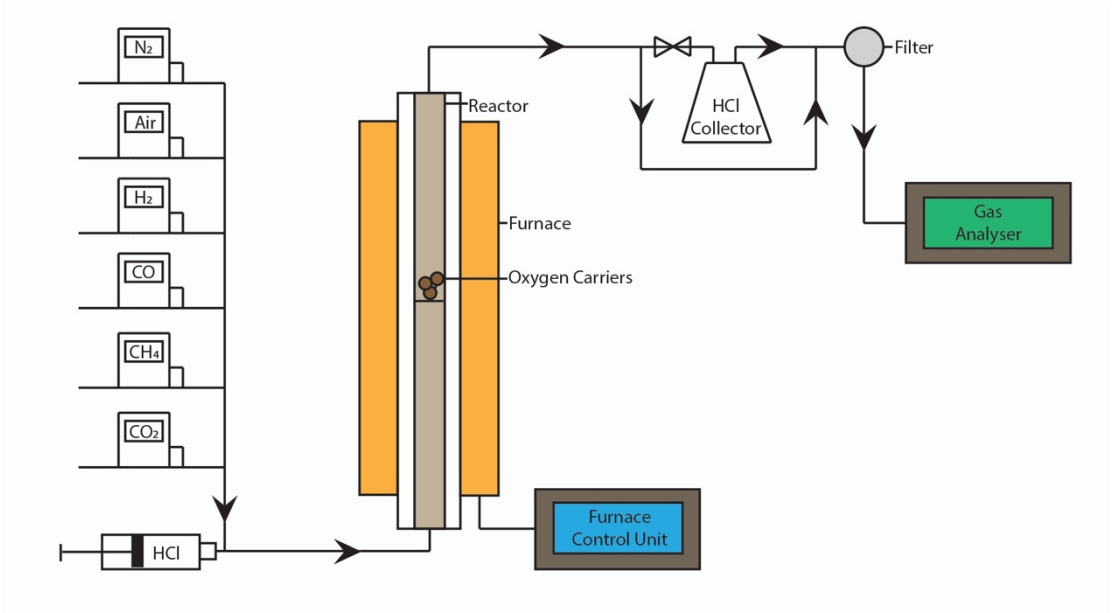

Fig.1 Experimental set up for CLC using a bench scale fluidized bed reactor

The gas switching program in one cycle was: N_2 (3 min, 400 ml/min) → simulated syngas (5 min, 375 ml/min) →N_2 (5 min, 500 ml/min) → air (4 min, 400 ml/min), in which simulated syngas was composed of 50 ml/min CO_2, 213 ml/min N_2, 50 ml/min CO, 50 ml/min H_2, 12 ml/min CH_4, and 0.14 ml/min HCl (1M) [26]. For each run, 10 g of OC was added into the reactor when testing FS and IO; for FS with α-Al_2O_3 as support, 10g of FS and 5g of α-Al_2O_3 was added. This combination is referred to as FS/Al_2O_3. 10 cycles were attempted for a basic CLC experiment; 50 cycles were attempted for an extended CLC experiment. The gaseous products were measured online by a gas analyzer (SICK, GME 810). The HCl content in the gaseous product was determined by collecting the condensate in the outlet, which was then measured by ion chromatography (IC, Thermo Fisher Dionex Aquion IC). To ensure evaporation of HCl into its gaseous form, the pipes leading to the reactor were heated up to 130 °C. The tests were triplicated to ensure that the results obtained were reproducible. The combustion efficiencies were presented based on their average values and with error bars to account for the standard deviations. The combustion efficiency of CO and H_2 and the removal efficiency of HCl were calculated as follows [27]:

$$\eta_{H_2} = \left(\frac{y_{in,H_2} - y_{out,H_2}}{y_{in,H_2}}\right) \times 100 \quad (1)$$

$$\eta_{CO} = \left(\frac{y_{in,CO} - y_{out,CO}}{y_{in,CO}}\right) \times 100 \quad (2)$$

$$E_{HCl} = \left(\frac{x_{in,HCl} - x_{out,HCl}}{x_{in,HCl}}\right) \times 100 \quad (3)$$

where η_{H_2} and η_{CO} are the combustion efficiencies for H_2 and CO respectively; E_{HCl} is the HCl removal efficiency; y_i is the molar concentration of species i as measured by the gas analyser; x_{HCl} is the mass concentration of HCl as measured by ion chromatography; the in subscript indicates the data obtained from the running the CLC with an inert bed; the out subscript refers to the data obtained from running the CLC with the OCs.

Thermogravimetric analysis (NETZSCH STA 449 F3 Jupiter) was performed to investigate the thermal properties of the OCs. This elucidated the oxygen transport capacity (OTC) of the OCs by subjecting them to reduction using H_2 (5% H_2/N_2, 210 ml/min) and oxidation using air (250 ml/min) at 850 °C. OTC was calculated by the mass loss under H_2 reduction. Additionally, H_2-temperature programmed reduction (H_2-TPR) of the OCs was also conducted using H_2 (5% H_2/N_2, 210 ml/min) from 100 °C to 900 °C (heating rate of 5 °C/min).

2.3 Characterization techniques

The elemental composition was analyzed using inductively coupled plasma – optical emission spectrometry (ICP-OES, Perkin Elmer Optima 8300) after microwave acid digestion (MAD, Multiwave 5000, Anton Paar). During MAD, 0.125g of OCs was digested by 3.6ml HNO_3, 1.8ml HCl and 1.2ml HF for 9.5min at 180 °C (heating rate of 18 °C/min). This was followed by de-complexation using 10ml H_3BO_3 for 20min at 150 °C (heating rate of 15 °C/min). The crystalline composition, morphology, surface area, and porosity of OCs were characterized by X-ray diffraction (XRD, Bruker D8 Advance), field emission scanning electron microscope with energy-dispersive X-ray spectrometer (FESEM-EDS, JSM-7200F with Oxford Aztec Standard X-max80, JEOL), Brunauer-Emmett-Teller (BET) and Barrer, Joiyner, and Halenda (BJH) method (Quadrasorb EVO/SI, Quantachrome Instrument) respectively.

2.4 Carbon footprint assessment

To evaluate the environmental impact of producing FS compared to IO, a carbon footprint assessment was conducted using the GaBi software and Ecoinvent 3.5 database. The boundary conditions for both IO and FS can be found in Fig. S1 while the mass and energy flow inventory for both OCs can be found in Table S1. The functional unit was 1 tonne of OC used in CLC.

The processes considered in this assessment include mining of iron ore, energy used in machinery needed for pre-treatment (sievers, crushers, and pelletizers), production and combustion of natural gas used for calcination, transportation of materials, landfill diversion from waste re-utilization, and waste streams generated during pre-treatment. All environmental burdens associated with the generation of FS by waterworks will be entirely allocated to the water treatment process. The impact categories chosen for comparison were global warming potential (100 years) (GWP-100) and global warming potential (20 years) (GWP-20). GWP-20 and GWP-100 refers to the amount of energy absorbed by the emissions of gases relative to CO_2 with a time range of 20 and 100 years respectively.

3 Results and discussions

3.1 Characterizations of fresh OCs

Table 1 shows the elemental composition of ferric sludge, FS, and IO. Fe content of the ferric sludge increased after calcination due to the decomposition of organics and removal of volatiles during calcination [28]. Comparison between IO and FS showed that IO has much higher amount of potentially active component with more Fe as compared to FS. On the other hand, FS contains higher amounts of potential complementary components such as Ca, Al, Si and Na oxides compared to IO.

Table 1 Elemental composition of ferric sludge, calcined ferric sludge and calcined iron ore.

Elements	Ferric Sludge Conc. ± (S.D.) (mg/kg)	FS OC Conc.± (S.D.) (mg/kg)	IO OC Conc.± (S.D.) (mg/kg)
Al	33,715.8± (4185.9)	94,674.6± (6354.1)	9489.2± (500.9)
As	23.4± (1.2)	61.9± (47.3)	31.5± (15.4)
Ba	99.3± (11.1)	228.6± (6.2)	129.6± (9.1)
Ca	149,443.2± (10,927.1)	326,358.3± (9100.4)	10,353.9± (836.8)
Cd	8.5± (2.1)	25.6± (16.8)	N.D.
Co	19.4± (2.1)	20.2± (8.1)	N.D.
Cr	230.0± (13.7)	636.1± (35.3)	359.7± (19.2)
Cu	85.9± (2.1)	156.0± (16.3)	N.D.
Fe	180,125.9± (11,674.3)	405,164.1± (9611.9)	706,001.1± (30226.3)
K	2225.9± (118.7)	4263.0± (40.4)	3873.9± (61.5)
Mg	14,521.9± (1057.2)	35,555.4± (550.8)	4791.9± (254.9)
Mn	1043.3± (64.0)	2244.5± (96.3)	3211.5± (169.3)
Mo	64.2± (2.1)	181.6± (32.0)	N.D.
Na	416.4± (130.4)	72,821.4± (2760.3)	4186.4± (190.3)
Ni	9.7± (4.2)	40.3± (7.0)	N.D.

Pb	59.2± (6.7)	156.0± (46.8)	N.D.
S	33,700.1± (4155.0)	5361.8± (631.9)	N.D.
Si	2874.6± (263.0)	41,245.3± (4620.0)	37,645.7± (1832.3)
Ti	682.6± (54.9)	1498.1± (19.1)	36,334.2± (2216.5)
V	66.6± (2.1)	123.7± (2.3)	901.0± (92.7)
Zn	2268.2± (137.3)	5076.7± (124.6)	823.5± (35.8)

*ND refers to the element concentration lower than detection limit (Cd <0.38mg/kg, Co <0.76mg/kg, Cu <1.52mg/kg, Mo <1.89mg/kg, Ni <1.89mg/kg, Pb <3.79mg/kg, and S <37.89mg/kg) of ICP-OES.

Fig. 2a shows the XRD patterns of FS, whereby the following ferric based oxide were detected, namely brownmillerite ($Ca_2Fe_2O_5$, COD 9014764), calcium iron oxide ($CaFe_2O_4$, COD 9013281), hematite (α-Fe_2O_3, COD 9015065) and maghemite (γ-Fe_2O_3, COD 9006316). In contrast to FS, only hematite was detected in IO. Therefore, maghemite and hematite are the main active phases for cyclic redox for FS while hematite is the main active phase for IO [29].

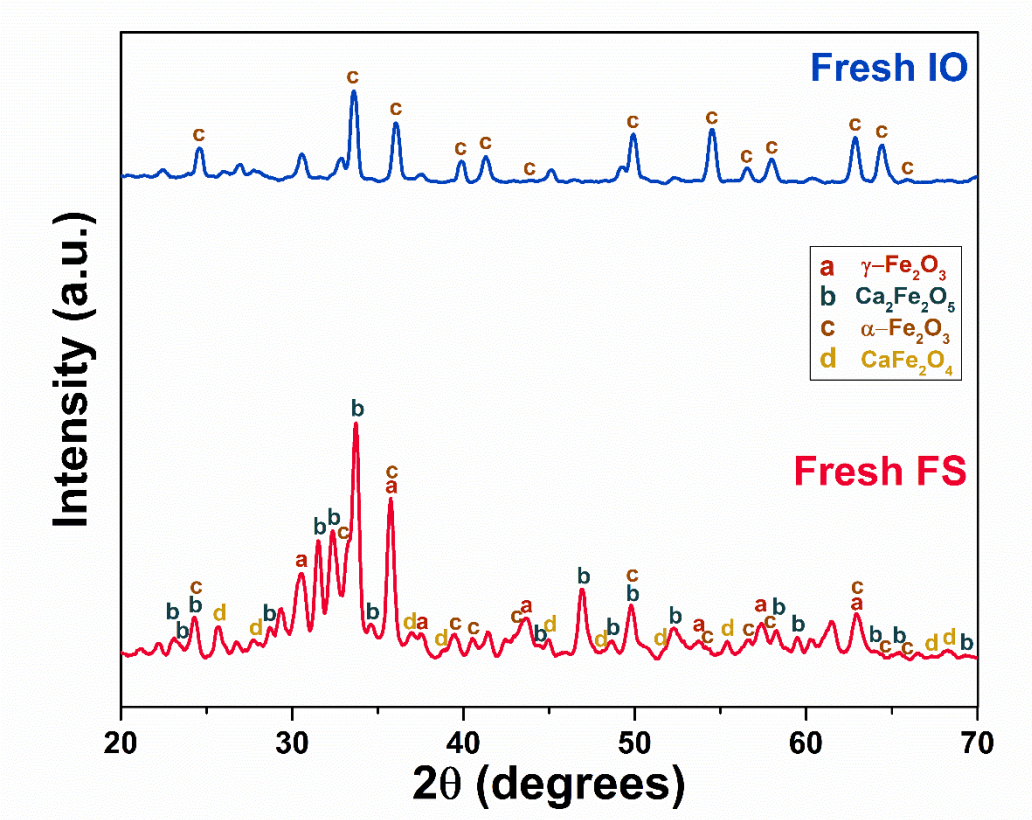

Fig. 2 XRD patterns of FS and IO after calcination elucidating the detected mineral phases of each OC

3.2 Redox reactivity of FS compared to IO

3.2.1 Redox activity

A comparison of OCs reactivity with syngas was further investigated; the results are shown in Fig. 3. Comparing the ferric content of both FS and IO, it would be expected that IO should

demonstrate better combustion efficiencies. However, as seen from Fig. 3a and 3b, FS performed better than IO in all 10 cycles. A minor decreasing trend was observed for FS in both CO and H_2 combustion efficiencies, whereby its capacity reduces as the cycles progress. In contrast, IO showed an increasing trend in performance. It was attributed to the activation effect [5], which improved the porosity of IO leading to higher performance.

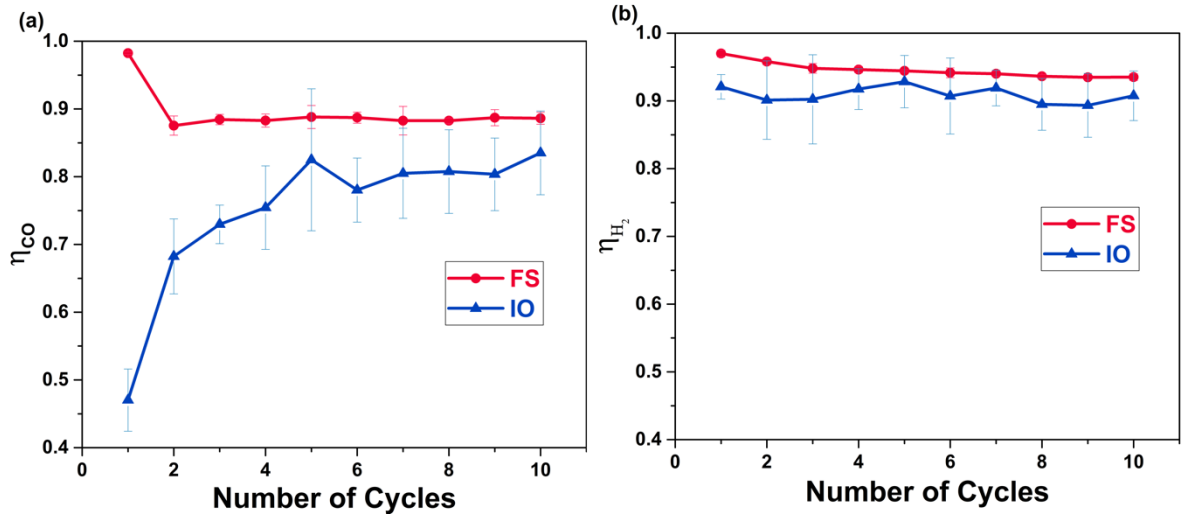

Fig. 3 (a) CO conversion efficiency using FS and IO as OC at 850 °C, (b) H_2 conversion efficiency using FS and IO as OC at 850 °C

Physical structure was characterized to further discuss the reactivity difference between FS and IO. The FESEM images in Fig. 4 shows that fresh and spent FS is more porous than fresh and spent IO. FS surface also contains the major elements of Fe and Ca as compared to only Fe for IO. Coupled with the data obtained from the BET results in Table 2, it can be observed that the surface area of fresh FS is approximately 43 times higher than IO while spent FS has approximately 5 times higher surface area compared to spent IO. High surface area and porous structures facilitates diffusion of fuel gas into the OC, thereby enhancing the reaction between the gas and solid surface, resulting in higher reactivity [30].

Lastly, FS contained considerably higher quantities of alkaline metals (i.e. Ca, Mg) than IO (Table 1 and Fig. 4a and 4c). Alkaline earth metal species can act as an electron donor to improve the lattice oxygen mobility of ferric oxide, thereby enhancing the reducibility [31]. This had been demonstrated by Liu, et al. [20], whereby IO modified with different alkaline earth metals (Ca, Ba, and Sr) showed improved combustion efficiencies during CLC. IO coated with Ca, Ba, and Sr obtained CO and H_2 combustion efficiencies of 89% and 95%, 95% and

96%, 95% and 96% respectively, as compared to pure IO of 77% and 86%. Furthermore, the fifth cycle performance of FS was similar to IO coated with Ca, achieving 89% and 94% for CO and H_2 combustion efficiency, which was attributed to the naturally high amount of Ca in FS. Overall, FS performed better than IO in terms of combustion efficiencies of CO and H_2, owing to its higher surface area and quantities of alkaline metals.

Table 2 BET Surface Area and BJH Pore Volume for the OCs

OCs	BET Surface Area (m^2/g)	BJH Pore Volume (ml/g)
IO	0.144	0.0009
IO (10 cycles)	0.398	0.0012
FS	6.303	0.0220
FS (10 cycles)	2.143	0.0034

To determine the competitiveness of FS as OC, its combustion efficiencies were compared against other waste materials. FS was able to achieve a high average combustion efficiency of 95% for H_2 and 89% for CO over 10 cycles. This result was similar to Yin, et al. [3], whereby the magnetic portion of the incineration bottom ash achieved combustion efficiencies of 95% and 90% for H_2 and CO respectively. The use of copper converter slag by Durmaz, et al. [8] also achieved high combustion efficiency of syngas (1:1 CO and H_2) of 89% which was similar to FS at 92% (average combustion efficiency of H_2 and CO). Thus, it can be concluded that FS is as competitive as these other waste materials as OCs in CLC, based on their similarly high combustion efficiencies.

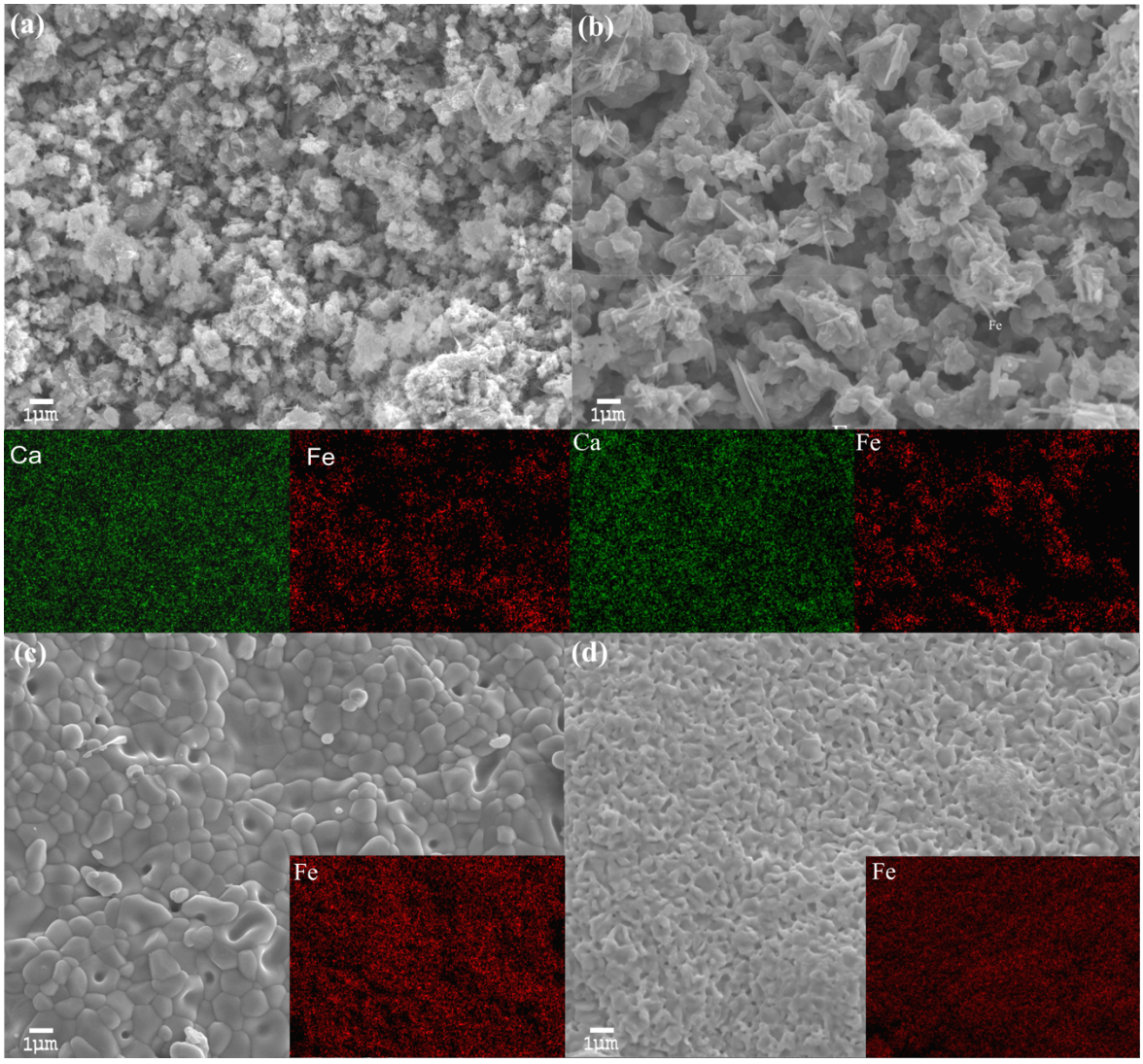

Fig. 4 (a) FESEM-EDS image of FS before CLC, (b) FESEM-EDS image of FS after CLC at 850 °C, (c) FESEM-EDS image of IO before CLC, (d) FESEM-EDS image of IO after CLC at 850 °C

3.2.2 HCl removal

The use of MSW syngas as the fuel source meant that the fuel contains acidic impurities like HCl, which are detrimental to the CLC process because of corrosion and pollutant generation. CLC with OCs that rely on transitional metal oxides (i.e oxides of Fe, Ni, and Cu) are not able to effectively dechlorinate the syngas [20]. Therefore, IO which was mainly composed of ferric oxide was unable to effectively remove HCl since the reaction between ferric oxide and HCl cannot proceed spontaneously [32].

FS contained significant amount of Na and Ca, which are alkali metal and alkaline earth metal species known to be able to effectively adsorb and remove HCl [32, 33]. Possible reactions for the sorption process are:

$$CaFe_2O_4 + 2HCl \rightarrow CaCl_2 + H_2O + Fe_2O_3 \quad (4)$$

$$Ca_2Fe_2O_5 + 4HCl \rightarrow 2CaCl_2 + 2H_2O + Fe_2O_3 \quad (5)$$

$$2NaFeO_2 + 2HCl \rightarrow 2NaCl + H_2O + Fe_2O_3 \quad (6)$$

FS with its high surface area will aid in chemisorption by providing more sites for the above reactions to take place. As seen in Fig. 5, FS was effective in removing HCl, with an efficiency from 92% to 71% over 10 cycles of CLC. However, as the cycles progressed, the sorbent components were gradually saturated for HCl adsorption, which corresponds with the decreased adsorption efficiency [34]. Besides this, FS also underwent agglomeration. The formation of NaCl and $CaCl_2$, which have low melting temperatures (801 °C and 774 °C, respectively) can exacerbate the reduction in adsorption efficiency [35]. In addition, the higher soluble chloride content of FS (286.43 mg/kg) compared to IO (3.55 mg/kg) could result in increased generation of molten products. The molten products would block the pores and agglomerate the particles which reduced the surface area available for chemisorption, thus resulting in a decrease in removal efficiency of HCl by FS. This may also contribute to the decreased in reactivity with syngas due to the decrease in surface area and sites available for reduction of OC to take place.

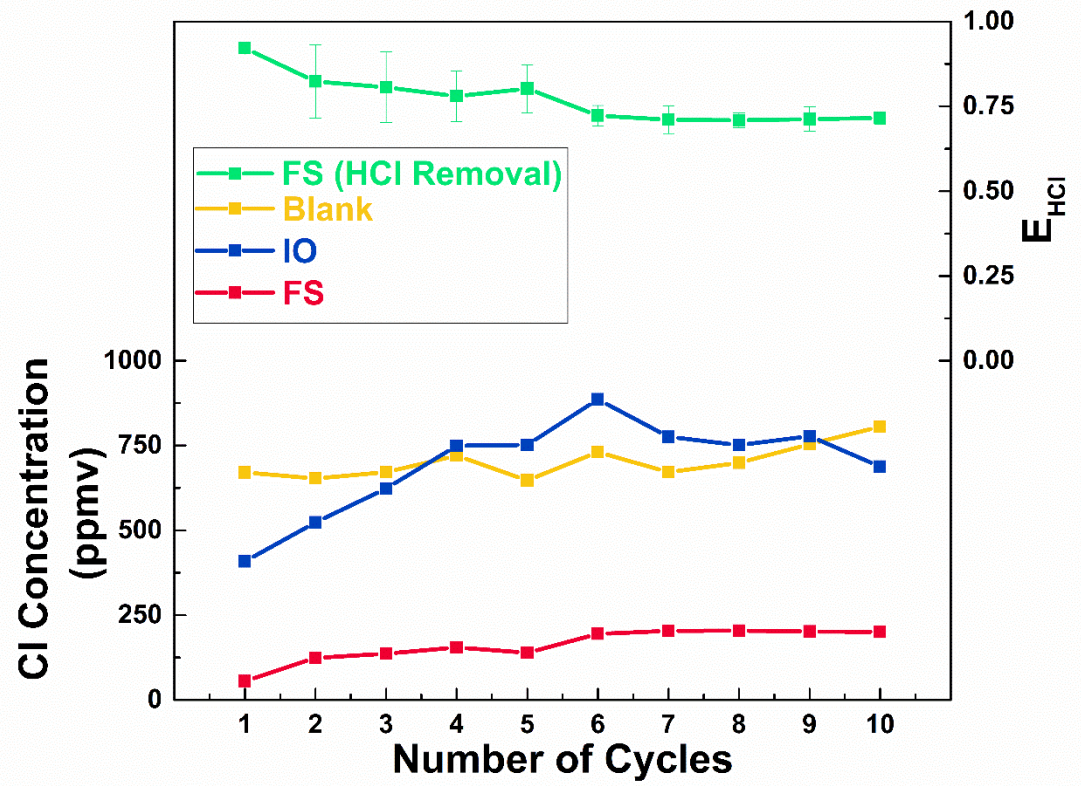

Fig. 5 HCl concentrations of flue gas during 10 cycles and HCl removal efficiency of FS during CLC

Interesting comparisons can be made on the HCl removal performance of FS compared to other materials in literature. In this study, FS had a removal efficiency of 92% which deteriorated to 71% over 10 cycles of CLC. This result is similar to Zhao, et al. [36], where their bifunctional alumina based sorbent achieved a removal efficiency of ~88% to ~71% for HCl after an hour of simultaneous removal of HCl and alkali metals. However, for sole removal of HCl, Cao, et al. [37] research on Ca-Mg-Al mixed oxides achieved ~95% removal efficiency throughout 200 minutes. Even though the initial removal efficiency of FS is similar, the performance of FS over time is lower in comparison. Nevertheless, due to its high initial removal efficiency, FS is a possible contender for the removal of acidic vapors. Further research focusing on HCl removal and adsorption, along with desorption of FS should be explored to determine its competitiveness in the removal of acidic vapors.

3.2.3 Transformation of OCs during CLC

The crystal phases of FS before and after CLC are shown in Fig. 6. It can be seen that the reduced FS mainly contained wüstite (FeO, COD 1011164) and brownmillerite ($Ca_2Fe_2O_5$). This suggests that the OC was not fully reduced to Fe^0, owing to the presence of steam in the syngas. With the presence of steam, $CaFe_2O_4$ tended to convert to $Ca_2Fe_2O_5$ [38], and FeO. Cho, et al. [39] discovered that severe agglomeration happened when iron oxide was reduced to the point where wüstite was formed, due to wüstite having a lower melting point compared to Fe_2O_3. After 10 redox cycles, the FS was mainly composed by Fe_2O_3 and $Ca_2Fe_2O_5$. It indicates that the $CaFe_2O_4$ was not recovered during multiple redox cycles, and the lower reactivity of $Ca_2Fe_2O_5$ with CO and H_2 could be the reason for the decline in OC reactivity [40].

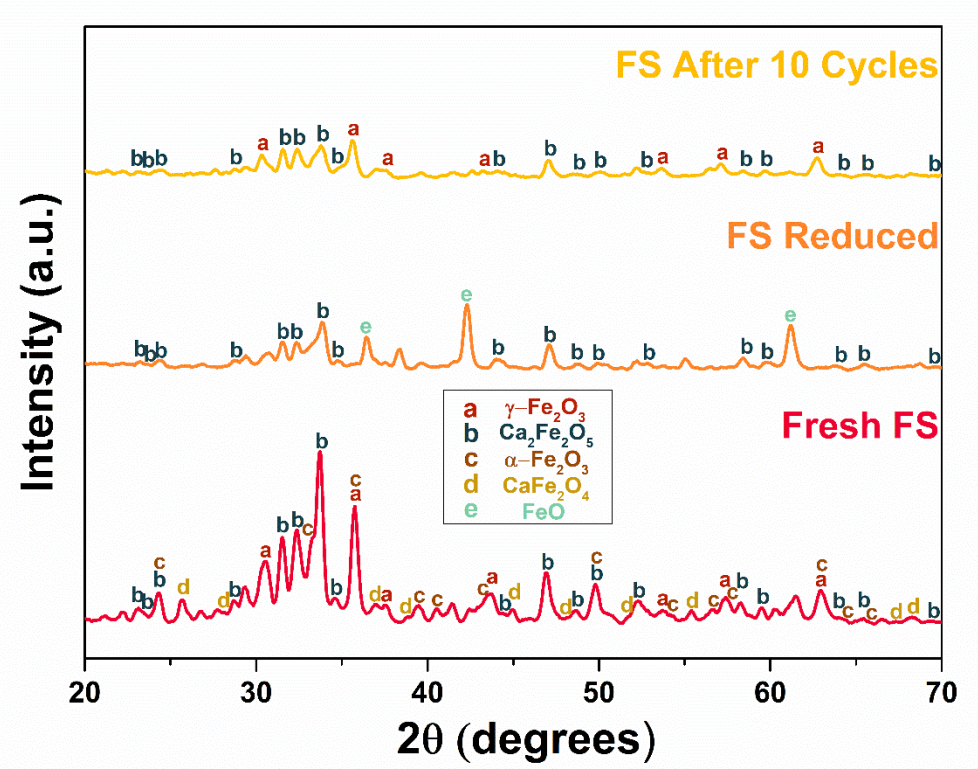

Fig. 6 XRD of FS at different conditions indicating how the mineral structure changes during CLC

The activity of OCs is also reflected by their reducibility, as characterized by H_2-TPR, as shown in Fig. 7a. The peaks of both the fresh IO and IO after 10 cycles were higher than the fresh FS and FS after 10 cycles, owing to the higher Fe content in IO. Both the fresh IO and IO after 10 cycles show a main reduction peak between 500°C and 600°C corresponding to the reduction of Fe_2O_3 to Fe_3O_4, and a small shoulder peak between 700°C and 750°C, which corresponds to the reduction of Fe_3O_4 to FeO and Fe [41]. TPR peaks of IO after 10 cycles were shifted to lower temperatures which indicates increased reduction rates and is thereby congruent with the CLC results obtained in Fig. 3 [1]. Conversely for FS, a shoulder peak between 450°C to 550°C and a main reduction peak between 600°C and 700°C were observed for both the fresh FS and FS after 10 cycles, which were attributed to the reduction of Fe_2O_3 to Fe_3O_4 and Fe_3O_4 to FeO, respectively [42]. Another shoulder peak beyond 850°C exhibited by both the fresh FS and FS after 10 cycles could be related to the reduction of brownmillerite [43]. Furthermore, the fresh FS has an additional shoulder peak between 650°C to 750°C that was absent for FS after 10 cycles, which is due to the reduction of $CaFe_2O_4$ [43]. TPR peaks of the FS after 10 cycles were also shifted to higher temperatures which indicates a decrease in reduction rates as seen from the CLC results in Fig. 3. The TPR results also suggests that interaction among various components in FS enhanced its reducibility compared to IO.

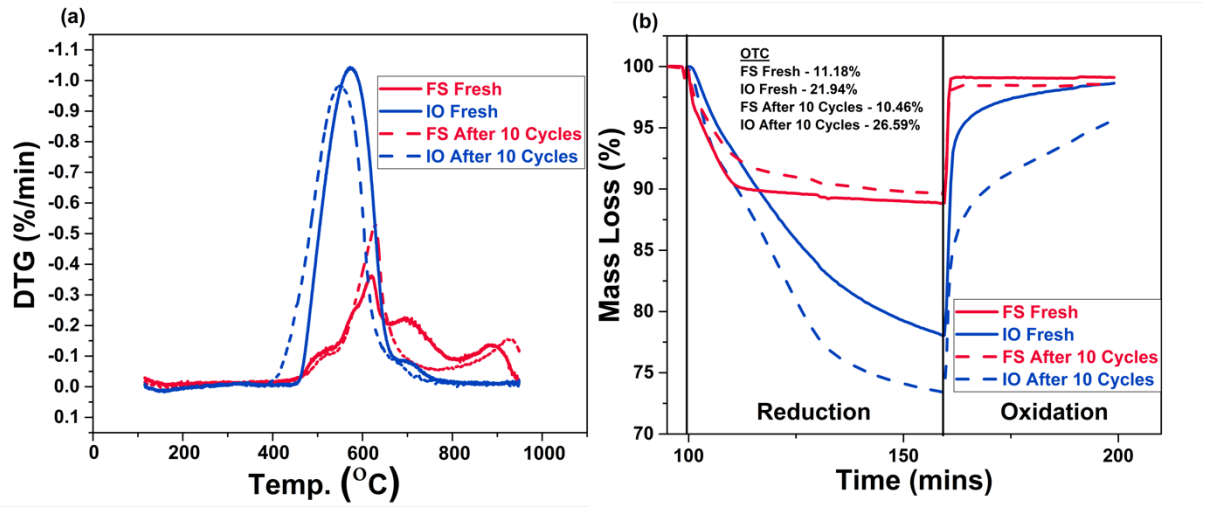

Fig. 7 TGA profiles of OCs: (a) H_2-TPR; (b) isothermal H_2 reduction at 850 °C

The TGA profiles of OCs in isothermal H_2 reduction are shown in Fig. 7b. The fresh FS had an oxygen transport capacity (OTC) of 11.18%, which was higher than FS after 10 cycles but lower than both the fresh IO and IO after 10 cycles. Furthermore, the fresh FS had the highest rate of reduction. This indicates that FS performance in CLC deteriorated as the cycles progress. Conversely, IO after 10 cycles had the highest OTC of 26.59 wt% and a higher rate of reduction than fresh IO, which meant that IO performance in CLC improves as the cycles progress. These findings are congruent with the CLC results shown in Fig. 3. However, it was observed that the oxidation rate of FS was greater than IO, with no deterioration between the fresh FS and FS after 10 cycles. On the other hand, IO after 10 cycles had a drastically reduced rate of oxidation as compared to the fresh IO; this tendency might eventually hinder IO's performance as more cycles progressed.

Table 3 shows the elemental compositions of both OCs before and after CLC. FS experienced more noticeable changes in elemental concentration than IO. Notably, there was a reduction of Na in FS after CLC, which can be attributed to the formation and partial evaporation of chloride salts due to high operating temperatures [35] and vaporization of Na and its compounds. The formation and melting of chloride salts also resulted in agglomeration of FS OCs [35]. Sulfur was also mostly removed during CLC, which is due to the vaporization of the sulfur element and compounds [44]. These high operating temperature may also lead to some vaporization of heavy metal compounds containing Pb and Cd during CLC as observed from the results [45]. The vaporization and elimination of these compounds and elements also increased the concentration of the remaining elements in the OC, as shown in Table 3.

While the transformation of heavy metals from FS to the gas phase might increase the burden of flue gas cleaning, the removal of hazardous components from the OC could potentially allow for further utilization of the spent FS as construction materials to achieve circularity of FS. $Ca_2Fe_2O_5$ that was found in FS could also be used as catalysts for water treatment too [46]. These findings indicated that CLC, together with appropriate flue gas cleaning processes, could be a potential pre-treatment step for the valorization of FS, thereby enabling the closing of the FS waste loop.

Table 3 Characterization of ferric sludge and iron ore before and after CLC

Elements	FS Conc. ± (S.D.) (mg/kg)	FS (after CLC) Conc. ± (S.D.) (mg/kg)	IO Conc. ± (S.D.) (mg/kg)	IO (after CLC) Conc. ± (S.D.) (mg/kg)
Al	94,674.6 ± (6354.1)	114,034.5 ± (27,724.2)	9489.2 ± (500.9)	10,225.9 ± (286.2)
As	61.9 ± (47.3)	276.6 ± (55.0)	31.5 ± (15.4)	N.D.
Ba	228.6 ± (6.2)	308.2 ± (70.1)	129.6 ± (9.1)	166.2 ± (3.7)
Ca	326,358.3 ± (9100.4)	504,181.9 ± (118,916.3)	10,353.9 ± (836.8)	9568.7 ± (524.8)
Cd	25.6 ± (16.8)	N.D.	N.D.	N.D.
Co	20.2 ± (8.1)	N.D.	N.D.	N.D.
Cr	636.1 ± (35.3)	958.6 ± (182.0)	359.7 ± (19.2)	699.1 ± (72.5)
Cu	156.0 ± (16.3)	376.4 ± (182.4)	N.D.	N.D.
Fe	405,164.1 ± (9611.9)	567,583.5 ± (113,821.6)	706,001.1 ± (30,226.3)	1,056,195.3 ± (33,213.2)
K	4263.0 ± (40.4)	4448.2 ± (506.3)	3873.9 ± (61.5)	3979.4 ± (57.4)
Mg	35,555.4 ± (550.8)	52,375.8 ± (11,727.0)	4791.9 ± (254.9)	4239.1 ± (256.3)
Mn	2244.5 ± (96.3)	3225.7 ± (740.8)	3211.5 ± (169.3)	3649.5 ± (65.7)
Mo	181.6 ± (32.0)	N.D.	N.D.	N.D.
Na	72,821.4 ± (2760.3)	5740.3 ± (776.8)	4186.4 ± (190.3)	4194.8 ± (223.0)
Ni	40.3	N.D.	N.D.	N.D.

	± (7.0)			
Pb	156.0 ± (46.8)	N.D.	N.D.	N.D.
S	5361.8 ± (631.9)	N.D.	N.D.	N.D.
Si	41,245.3 ± (4620.0)	113,087.3 ± (25,864.1)	37,645.7 ± (1832.3)	33,852.2 ± (2432.3)
Ti	1498.1 ± (19.1)	2168.5 ± (498.3)	36,334.2 ± (2216.5)	33,586.3 ± (96.0)
V	123.7 ± (2.3)	N.D.	901.0 ± (92.7)	1601.3 ± (65.3)
Zn	5076.7 ± (124.6)	5639.2 ± (1271.6)	823.5 ± (35.8)	1095.5 ± (22.3)

*ND refers to the element concentration lower than detection limit (As <3.79mg/kg, Cd <0.38mg/kg, Co <0.76mg/kg, Cu <1.52mg/kg, Mo <1.89mg/kg, Ni <1.89mg/kg, Pb <3.79mg/kg, and S <37.89mg/kg) of ICP-OES.

3.3 Reactivity of FS in CLC under different operating temperatures

The reactivity of FS under different temperatures was investigated to evaluate the sensitivity of the CLC performance as a function of the redox temperature. Redox cycles were performed in 3 different temperatures of 800 °C, 850 °C, and 900 °C as shown in Fig. 8a and 8b. There were marginal differences between the combustion efficiencies at 800 °C and 850 °C, while the combustion efficiencies were lower at 900 °C.

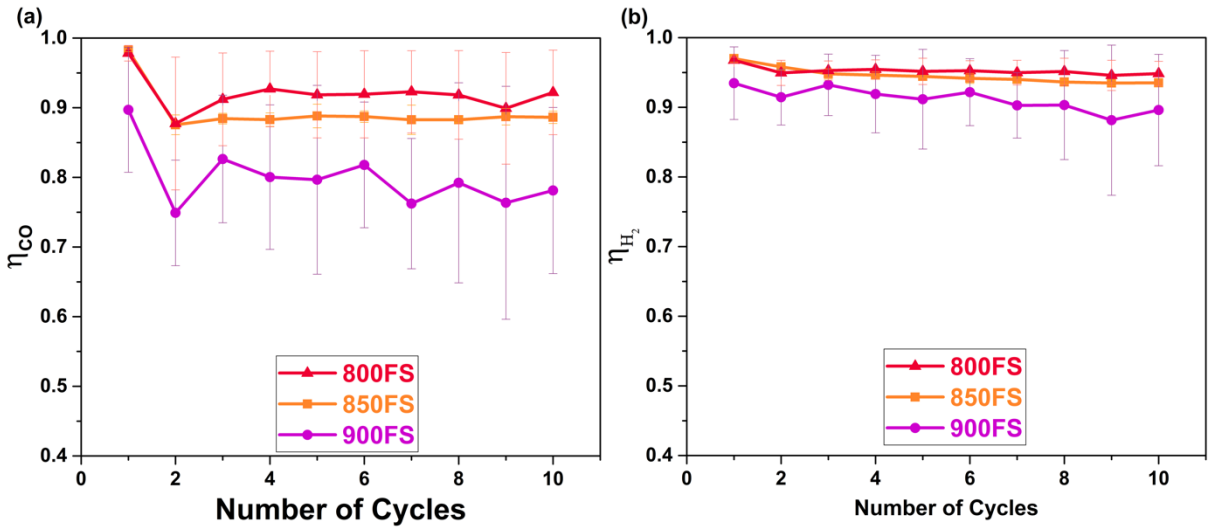

Fig. 8 (a) CO conversion efficiency using FS as OC at different temperatures, (b) H_2 conversion efficiency using FS as OC at different temperatures

However, for other types of OCs, higher fuel reactor temperature usually led to the higher conversion of fuels [47]. This suggests that changes in the physical properties of FS may have

affected their performance at higher reactor temperatures. Fig. S2 shows how the morphology of FS changed after CLC at different temperatures, as observed by FESEM. The FS after CLC at 900 °C seems to experience more agglomeration than at the other 2 temperatures. Agglomeration reduced the surface contact with the syngas, therefore reducing the reactivity and combustion efficiencies during CLC [48]. Thus, the optimal CLC temperature for using FS as an OC for CLC will be between 800°C to 850°C. This means the fuel reactor does not have to be maintained at higher temperature during CLC operation with FS as the OC.

3.4 Reactivity in extended cycles

The redox tests of FS during extended cycles were discontinued owing to the severe agglomeration (shown in Fig. S3a). To address the agglomeration issue, α-Al_2O_3 was employed to stabilize the oxygen carrier to hinder the sintering of the active components. The mass ratio of FS to α-Al_2O_3 used was 2:1 (10 g FS and 5 g α-Al_2O). Also, α-Al_2O_3 might prevent the agglomeration from molten alkali metal salts through the formation of mixed metal oxides (e.g., $NaAlO_2$ and $KAlO_2$) [49]. As expected, the addition of α-Al_2O_3 to FS drastically reduced agglomeration between FS particles, as shown in Fig. S3b. The prevention of sintering, i.e. reduced agglomeration between the grains, enhances the stability of FS OC, which allowed for the stable operation in extended redox cycles. However, minor agglomeration still occurred on the FS particle surface as seen in Fig. 9a and 9b for FS/Al_2O_3.

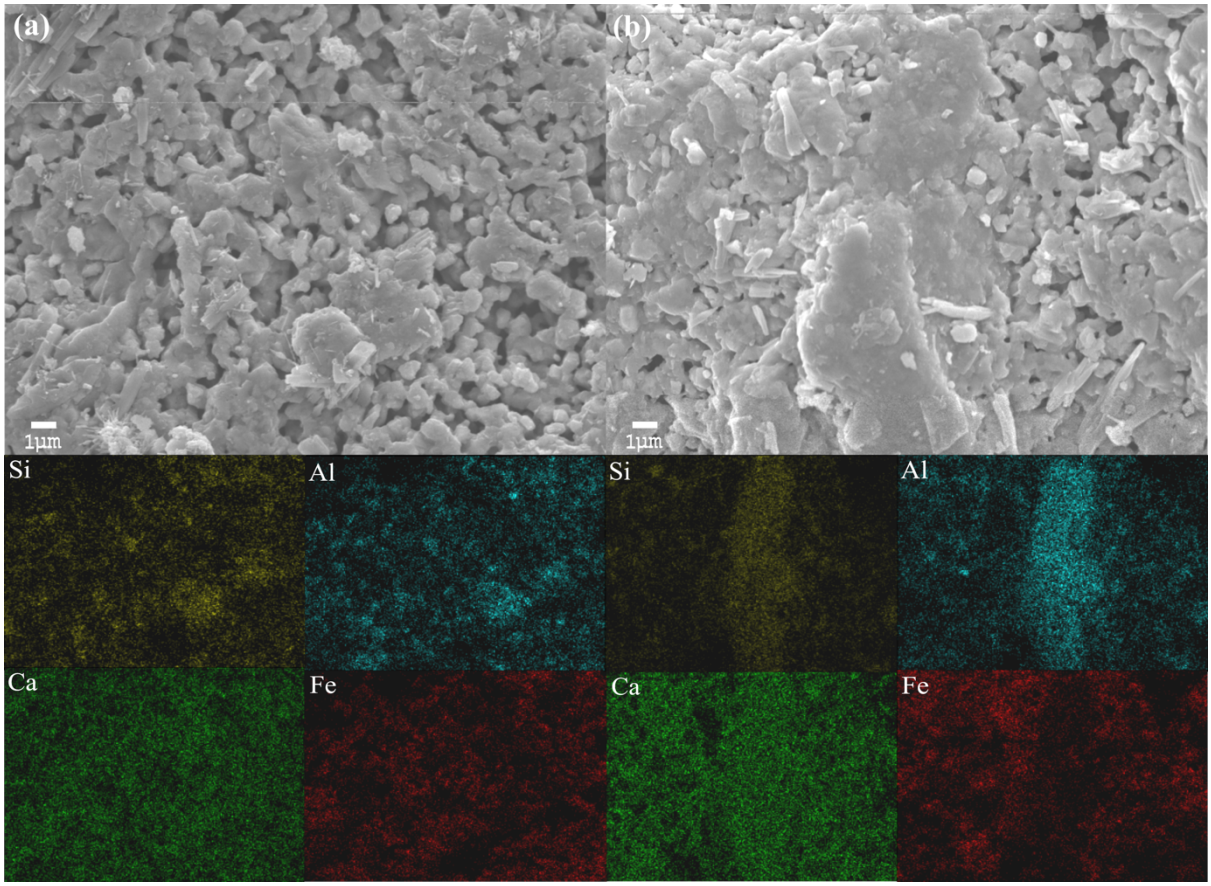

Fig. 9 FESEM-EDS images of FS in the FS/Al_2O_3 OC after (a) 10 cycles and (b) 50 cycles

The performance of diluted FS (FS/Al_2O_3) throughout 50 successive cycles is shown in Fig. 10. The conversion efficiency demonstrated a decreasing trend when FS/Al_2O_3 was used as the OC. Interestingly, there was a steep decrease for the first few cycles followed by a gradual plateau for the remaining cycles, achieving the lowest CO combustion efficiency of 70% and 86% for H_2. Fig. S4a, S4b, and S4c shows the raw data collected by the analyzer whereby a stark difference between the first and 25th cycle was seen, while the difference between 25th cycle and 50th cycle was almost negligible.

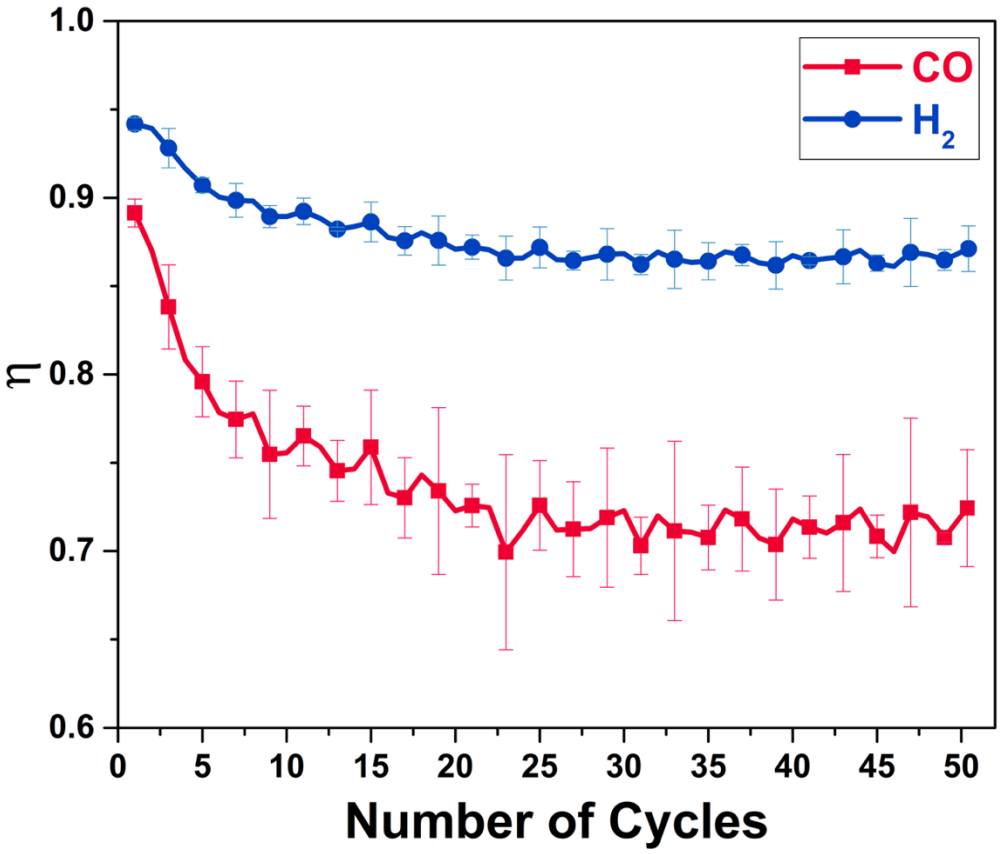

Fig. 10 CO and H_2 conversion efficiency using FS/Al_2O_3 as OC at 850 °C for 50 cycles CLC

The trend can be explained by the agglomeration behavior of the OC. The specific surface area and pore volume of the OCs between 10^{th} and 50^{th} cycles were similar as seen in Table 4. Thus, the steep decrease in efficiency can be attributed to the particle surface rapidly sintering during the first 10 cycles, while further sintering beyond 10 cycles was efficiently alleviated by the Al_2O_3 support. The initial deactivation was also accompanied by the irreversible transformation of $CaFe_2O_4$ into $Ca_2Fe_2O_5$, which has lower reactivity with CO and H_2 than $CaFe_2O_4$ [40]. At the start of the cycles, $CaFe_2O_4$ and $Ca_2Fe_2O_5$ contributed to the higher combustion efficiencies, but as the cycles progressed, more $CaFe_2O_4$ was converted to $Ca_2Fe_2O_5$, resulting in decreasing combustion efficiencies.

Table 4 BET Surface Area and BJH Pore Volume for OCs undergoing extended cycles

OCs Samples	BET Surface Area (m^2/g)	BJH Pore Volume (ml/g)
FS/Al_2O_3 (10 cycles)	0.888	0.002
FS/Al_2O_3 (50 cycles)	0.891	0.001

The addition of α-Al_2O_3 allowed for an extended CLC operation. However, it will also affect the reactivity of the FS OC. This was demonstrated in Fig. 10 and Fig. 3, where FS outperformed FS/Al_2O_3 during the first 10 cycles. The formation of irreversible silicates led to reduced reactivity. Silicates were formed on the surface of FS, where Si from FS reacts with Al from α-Al_2O_3 evident in Fig. 9a and 9b [50]. This hampered the diffusion of the fuel gas into the OC, thus reducing reactivity. While this impacted the CO combustion efficiency, the difference in H_2 combustion efficiency between FS/Al_2O_3 and FS was minimal. Therefore, the addition of α-Al_2O_3 improved the stability of the OC by preventing agglomeration, though at the cost of slightly reducing combustion efficiencies during CLC.

3.5 Comparing carbon footprints of using IO and FS as oxygen carrier

The global warming potentials (GWP-20 and GWP-100) of FS and IO, excluding biogenic carbon, were shown in Fig. 12. GWP-20 and GWP-100 for the conversion of FS to an OC for CLC of syngas are 427.87 and 370.90 kgCO_2/t, respectively. This is lower than the utilization of IO as the OC which contributed 532.10 and 478.90 kgCO_2/t towards GWP-20 and GWP-100 respectively. The calculated GWP excluded the transport of materials within the city (where the CLC of MSW syngas is applied) as it is assumed to be similar for both IO and FS for simplicity. Therefore, this assessment of the carbon footprints of FS and IO demonstrated the competitiveness of converting wastes into useful products as compared to the mining of natural resources.

The detailed component analysis revealed that due to the additional pre-treatment step of pelletizing, as illustrated in Table S1, the electricity usage for producing FS was higher than IO, which contributed towards both GWP indicators. Heat is necessary for both drying of ferric sludge due to its high water content seen in Table S1 and calcination of ferric sludge into a usable OC. Conversely only calcination is required for IO. This meant that the CO_2 emitted from combustion of natural gas and the amount of natural gas used for FS was higher than IO. Generally, GWP-20 for both IO and FS were higher than GWP-100 due to the fact that CH_4 GWP-20 was ~3 times more than GWP-100 [51]. This is because CH_4 absorbs significantly more energy than CO_2 but has a much shorter lifespan of 12.4 years [52]. Since natural gas production resulted in emissions of fossil CH_4, this explained the significant difference between its GWP-20 and GWP-100 values for both IO and FS [53]. Nevertheless, considering

that the OCs will be applied in a MSW gasification plant, it is possible to replace the use of natural gas with heat generated from the waste treatment process itself for the calcination. This could further reduce the carbon footprint of both OCs. Although the diversion of heat would potentially reduce the net electricity generated from the MSW gasification plant, the synergistic production and utilization of OCs on site with the heat from the waste treatment process will be beneficial in lowering the net carbon footprints.

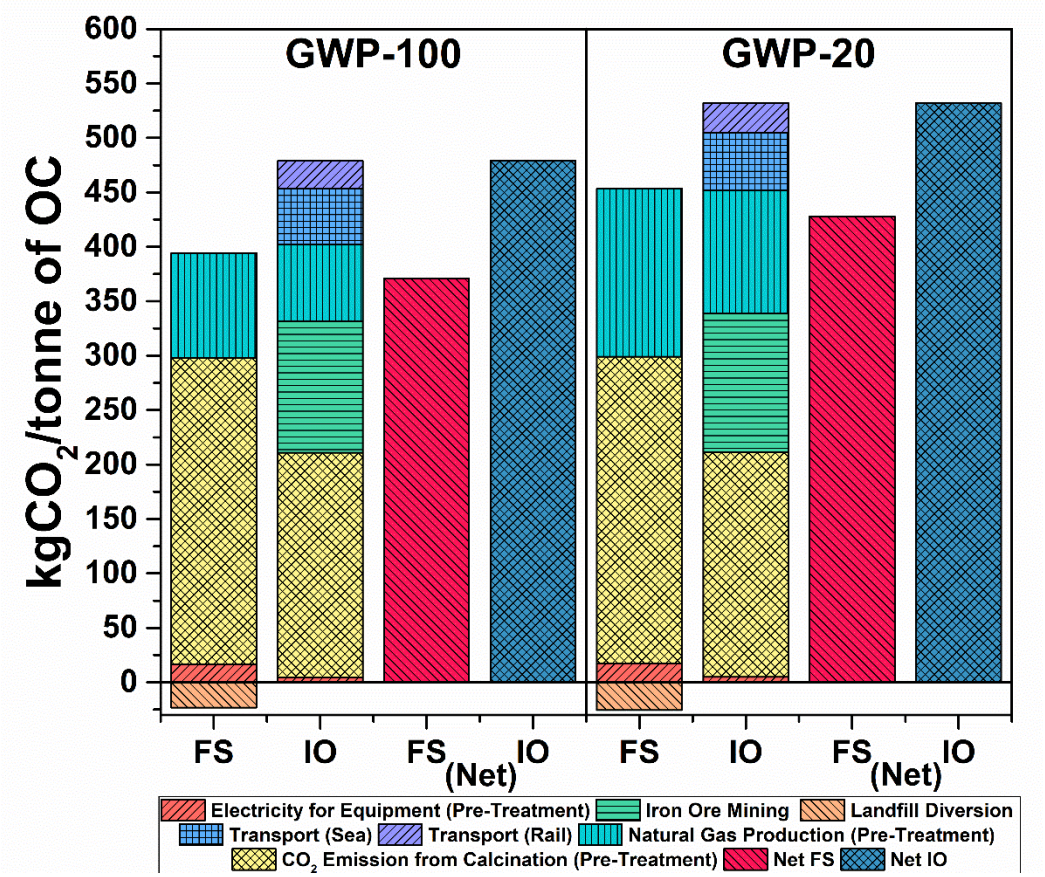

Fig. 12 Carbon footprint of FS and IO for use as OC. The individual component breakdown for both GWP-100 and GWP-20 are presented as the first and second bars for FS and IO respectively. Net carbon footprint for GWP-100 and GWP-20 are presented as the third and fourth bars for FS and IO respectively.

As FS is a waste (or a by-product) generated from the water treatment facility, which is usually located in a city, there is no additional transportation needed. Conversely for IO, a weighted average distance on the imports of iron ore from the top three exporters (Australia, Sweden and South Africa) to the targeted cities was used to calculate the impacts from rail and sea transport [54] respectively, which was described in Table S2. The rail transport refers to the movement of iron ore from the mine to the port, while the sea transport refers to the transboundary movement of iron ore from the country of origin to the country that imported it. This resulted in increased emissions for both GWP-100 and GWP-20 for using IO as an oxygen carrier.

IO is the product of traditional mining, which uses the linear approach of "take-make-waste". Even though it is more abundant and cheaper compared to other types of ores, the mining of IO is still energy intensive [55]. On the other hand, FS is the by-product generated from the freshwater treatment and can be recovered through urban mining. Urban mining is when compounds or elements of interest (ferric oxides, alkaline earth metals, and alkali metals) are reclaimed from an anthropogenic stock (water treatment waste stream) and thus achieving circularity [56]. This allowed for the "mining" of resources from a waste stream, thus generation of sludge was not included in the carbon footprint assessment. The re-utilization of sludge led to landfill diversion of FS which resulted in negative contribution towards GWP.

As the world becomes more environmentally conscious, new innovations and solutions must be sustainable to reduce environmental impacts. The carbon footprint assessment allowed for the effective comparison of a new solution against established procedures based on their carbon emissions. Coupled with performance and cost evaluation, this provides a comprehensive comparison between them and will ensure that a more informed decision will be made on adopting new solutions over established ones. Therefore, the inclusion of a carbon footprint assessment for new reengineering solutions should be encouraged.

To contribute towards improving the circularity of the CLC process, spent OCs should be further repurposed or reused to prevent landfilling of these spent materials. These include metals recovery such as Cu extraction from Cu-based OC [57], or smelting for iron production from spent IO as both forms of Fe (Fe_2O_3 and Fe_3O_4) are present [58]. For using FS as OC, the potential of reusing spent FS in the construction industry is promising. This is because of its relatively high Ca, Si, and Al contents, which can potentially be applied as additive or supplementary cementitious material to replace natural resources and to improve concrete properties [59]. Thus, the usage of FS in CLC and subsequently in the construction industry can ensure circularity of ferric sludge while maximizing its value and should be further studied in future works.

To further assess the self-sufficiency of using ferric sludge as an OC in a city, the utilization rate and production capacity are assessed. Considering a commercial gasifier (functional unit) with a typical capacity of 300 t/day of MSW, the syngas generated is approximately 810,000 Nm^3/day based on the estimated syngas yield of 2.7 Nm^3/kg [26]. Assuming the optimized OC

applied can be reused for at least 200 cycles, the amount of OC needed is around 6.75 t/day based on its OTC [60]. As the amount of waterworks sludge generated from the waterworks in a city is generally around 40 to 60 t/day [61], this will result in the generation of approximately 18.5 to 27.7 t/day of FS after the pre-treatment for OC production. Therefore, it is expected that the FS generated in a city is sufficient to be applied in CLC for multiple (~4) commercial-scale gasifiers.

4 Conclusion

Treated ferric sludge is deemed to be an effective OC for application in chemical looping syngas combustion. Using FS as an OC allows for lower CLC operating temperature while affording high combustion efficiencies. Compared to iron ores, FS performed better over 10 CLC cycles in a fluidized bed using simulated MSW syngas as the fuel. Besides this, FS could also simultaneously and effectively remove HCl during CLC. However, problems including sintering and agglomeration arose from the formation of low-melting chloride salts and reduction into wüstite. The addition of α-Al_2O_3 as a support in FS yielded good results as it drastically reduces the extent of sintering and agglomeration, while still achieving good combustion efficiencies. Comparison of the global warming potentials (GWPs) of IO and FS shows that FS-derived OC corresponds to reduced GWPs. Specifically, FS achieved 104.23 and 108.0 $kgCO_2/t$ less than IO for GWP-20 and GWP-100 respectively. This study unearthed the possibility of using FS as an oxygen carrier, which is a novel and sustainable direction for sludge reutilization.

References:

[1] H. Wang, X. Dou, A. Veksha, W. Liu, A. Giannis, L. Ge, T. Thye Lim, G. Lisak, Barium aluminate improved iron ore for the chemical looping combustion of syngas, Applied Energy 272 (2020). https://doi.org/10.1016/j.apenergy.2020.115236.

[2] W. Qin, S. Chen, B. Ma, J. Wang, J. Li, R. Liang, Z. Xu, L. Liu, C. Dong, H. Zhang, Methanol solution promoting cotton fiber chemical looping gasification for high H2/CO ratio syngas, International Journal of Hydrogen Energy 44 (2019) 7149-7157. https://doi.org/https://doi.org/10.1016/j.ijhydene.2019.01.267.

[3] K. Yin, H. Wang, A. Veksha, X. Dou, D. Khairunnisa Binte Mohamed, S. Heberlein, G. Liu, W. Chen, G. Lisak, Oxygen carriers from incineration bottom ash for chemical looping combustion of syngas: Effect of composition on combustion efficiency, Chemical Engineering Journal 405 (2021). https://doi.org/10.1016/j.cej.2020.127068.

[4] A. Lyngfelt, Chemical Looping Combustion: Status and Development Challenges, Energy & Fuels 34(8) (2020) 9077-9093. https://doi.org/10.1021/acs.energyfuels.0c01454.

[5] T. Mendiara, A. Abad, L.F. de Diego, F. García-Labiano, P. Gayán, J. Adánez, Reduction and oxidation kinetics of Tierga iron ore for Chemical Looping Combustion with diverse fuels, Chemical Engineering Journal 359 (2019) 37-46. https://doi.org/10.1016/j.cej.2018.11.022.

[6] Z. Gu, L. Zhang, C. Lu, S. Qing, K. Li, Enhanced performance of copper ore oxygen carrier by red mud modification for chemical looping combustion, Applied Energy 277 (2020). https://doi.org/10.1016/j.apenergy.2020.115590.

[7] S. Sundqvist, M. Arjmand, T. Mattisson, M. Rydén, A. Lyngfelt, Screening of different manganese ores for chemical-looping combustion (CLC) and chemical-looping with oxygen uncoupling (CLOU), International Journal of Greenhouse Gas Control 43 (2015) 179-188. https://doi.org/10.1016/j.ijggc.2015.10.027.

[8] M. Durmaz, N. Dilmaç, Ö.F. Dilmaç, Evaluation of performance of copper converter slag as oxygen carrier in chemical-looping combustion (CLC), Energy 196 (2020). https://doi.org/10.1016/j.energy.2020.117055.

[9] E. Ksepko, Sewage sludge ash as an alternative low-cost oxygen carrier for chemical looping combustion, Journal of Thermal Analysis and Calorimetry 116(3) (2013) 1395-1407. https://doi.org/10.1007/s10973-013-3564-7.

[10] Y.L. Kuo, W.C. Huang, Y.H. Tseng, S.H. Chang, Y. Ku, H.Y. Lee, Electric arc furnace dust as an alternative low-cost oxygen carrier for chemical looping combustion, J Hazard Mater 342 (2018) 297-305. https://doi.org/10.1016/j.jhazmat.2017.08.024.

[11] T. Mendiara, F. García-Labiano, P. Gayán, A. Abad, L.F. de Diego, J. Adánez, Evaluation of the use of different coals in Chemical Looping Combustion using a bauxite waste as oxygen carrier, Fuel 106 (2013) 814-826. https://doi.org/10.1016/j.fuel.2012.11.047.

[12] Z. Yu, Y. Yang, S. Yang, Q. Zhang, J. Zhao, Y. Fang, X. Hao, G. Guan, Iron-based oxygen carriers in chemical looping conversions: A review, Carbon Resources Conversion 2(1) (2019) 23-34. https://doi.org/10.1016/j.crcon.2018.11.004.

[13] P. Jarvis, E. Sharp, M. Pidou, R. Molinder, S.A. Parsons, B. Jefferson, Comparison of coagulation performance and floc properties using a novel zirconium coagulant against traditional ferric and alum coagulants, Water Research 46 (2012) 4179-4187. https://doi.org/doi:10.1016/j.watres.2012.04.043.

[14] D.I. Verrelli, D.R. Dixon, P.J. Scales, Effect of coagulation conditions on the dewatering properties of sludges produced in drinking water treatment, Colloids and Surfaces A: Physicochemical and Engineering Aspects 348(1-3) (2009) 14-23. https://doi.org/10.1016/j.colsurfa.2009.06.013.

[15] A.M. Hidalgo, M.D. Murcia, M. Gómez, E. Gómez, C. García-Izquierdo, C. Solano, Possible Uses for Sludge from Drinking Water Treatment Plants, Journal of Environmental Engineering 143(3) (2017). https://doi.org/10.1061/(asce)ee.1943-7870.0001176.

[16] M.D. Nguyen, M. Thomas, A. Surapaneni, E.M. Moon, N.A. Milne, Beneficial reuse of water treatment sludge in the context of circular economy, Environmental Technology & Innovation 28 (2022) 102651. https://doi.org/https://doi.org/10.1016/j.eti.2022.102651.

[17] B. Bağrıaçık, E.D. Güner, An Experimental Investigation of Reinforcement Thickness of Improved Clay Soil with Drinking Water Treatment Sludge as an Additive, KSCE Journal of Civil Engineering 24(12) (2020) 3619-3627. https://doi.org/10.1007/s12205-020-0111-5.

[18] M. Ismail, W. Liu, S.A. Scott, The performance of Fe2O3-CaO Oxygen Carriers and the Interaction of Iron Oxides with CaO during Chemical Looping Combustion and H2 production, Energy Procedia 63 (2014) 87-97. https://doi.org/10.1016/j.egypro.2014.11.010.

[19] H. Jiang, R. Huo, Z. Zhang, Y. Lin, Z. Zhao, J. Hu, Z. Huang, H. Huang, H. Li, Dechlorination performance in

chemical looping conversion of polyvinyl chloride plastic waste using K/Na/Ca-modified iron ore oxygen carriers, Journal of Environmental Chemical Engineering 10(2) (2022). https://doi.org/10.1016/j.jece.2022.107314.
[20] G. Liu, H. Wang, A. Veksha, A. Giannis, T.T. Lim, G. Lisak, Chemical looping combustion-adsorption of HCl-containing syngas using alkaline-earth coated iron ore composites for simultaneous purification and combustion enhancement, Chemical Engineering Journal 417 (2021). https://doi.org/10.1016/j.cej.2021.129226.
[21] G. Liu, Y. Liao, Y. Wu, X. Ma, Enhancement of Ca2Fe2O5 oxygen carrier through Mg/Al/Zn oxide support for biomass chemical looping gasification, Energy Conversion and Management 195 (2019) 262-273. https://doi.org/https://doi.org/10.1016/j.enconman.2019.04.087.
[22] R. Xiao, Q. Song, Characterization and kinetics of reduction of CaSO4 with carbon monoxide for chemical-looping combustion, Combustion and Flame 158(12) (2011) 2524-2539. https://doi.org/10.1016/j.combustflame.2011.05.011.
[23] N. Ding, Y. Zheng, C. Luo, Q.-l. Wu, P.-f. Fu, C.-g. Zheng, Investigation into compound CaSO4 oxygen carrier for chemical-looping combustion, Journal of Fuel Chemistry and Technology 39(3) (2011) 161-168. https://doi.org/10.1016/s1872-5813(11)60015-7.
[24] J.M. Guilemany, M. Torrell, J.R. Miguel, Study of the HVOF Ni-Based Coatings' Corrosion Resistance Applied on Municipal Solid-Waste Incinerators, Journal of Thermal Spray Technology 17(2) (2008) 254-262. https://doi.org/10.1007/s11666-008-9167-3.
[25] H. Zhou, A. Meng, Y. Long, Q. Li, Y. Zhang, A review of dioxin-related substances during municipal solid waste incineration, Waste Manag 36 (2015) 106-18. https://doi.org/10.1016/j.wasman.2014.11.011.
[26] W.P. Chan, A. Veksha, J. Lei, W.-D. Oh, X. Dou, A. Giannis, G. Lisak, T.-T. Lim, A hot syngas purification system integrated with downdraft gasification of municipal solid waste, Applied Energy 237 (2019) 227-240. https://doi.org/10.1016/j.apenergy.2019.01.031.
[27] F. Mayer, A.R. Bidwe, A. Schopf, K. Taheri, M. Zieba, G. Scheffknecht, Comparison of a new micaceous iron oxide and ilmenite as oxygen carrier for Chemical looping combustion with respect to syngas conversion, Applied Energy 113 (2014) 1863-1868. https://doi.org/10.1016/j.apenergy.2013.04.056.
[28] M.A. Tantawy, Characterization and pozzolanic properties of calcined alum sludge, Materials Research Bulletin 61 (2015) 415-421. https://doi.org/10.1016/j.materresbull.2014.10.042.
[29] T. Song, T. Shen, L. Shen, J. Xiao, H. Gu, S. Zhang, Evaluation of hematite oxygen carrier in chemical-looping combustion of coal, Fuel 104 (2013) 244-252. https://doi.org/10.1016/j.fuel.2012.09.030.
[30] H. Gu, L. Shen, J. Xiao, S. Zhang, T. Song, D. Chen, Evaluation of the Effect of Sulfur on Iron-Ore Oxygen Carrier in Chemical-Looping Combustion, Industrial & Engineering Chemistry Research 52(5) (2013) 1795-1805. https://doi.org/10.1021/ie303023w.
[31] H. Wang, G. Liu, A. Veksha, X. Dou, A. Giannis, T.T. Lim, G. Lisak, Iron ore modified with alkaline earth metals for the chemical looping combustion of municipal solid waste derived syngas, Journal of Cleaner Production 282 (2021). https://doi.org/10.1016/j.jclepro.2020.124467.
[32] J. Wang, H. Zhao, Chemical looping dechlorination through adsorbent-decorated Fe2O3/Al2O3 oxygen carriers, Combustion and Flame 162(10) (2015) 3503-3515. https://doi.org/10.1016/j.combustflame.2015.06.008.
[33] G. Liu, H. Wang, S. Deplazes, A. Veksha, C. Wirz-Töndury, A. Giannis, T.T. Lim, G. Lisak, Ba–Al-decorated iron ore as bifunctional oxygen carrier and HCl sorbent for chemical looping combustion of syngas, Combustion and Flame 223 (2021) 230-242. https://doi.org/10.1016/j.combustflame.2020.09.021.
[34] X. Ma, X. Huang, T. Feng, M. Mu, X. Hu, A DFT study on the mechanism of HCl and CO2 capture by CaO, Reaction Chemistry & Engineering 7(3) (2022) 758-768. https://doi.org/10.1039/d1re00487e.
[35] C. Sevonius, P. Yrjas, D. Lindberg, L. Hupa, Impact of sodium salts on agglomeration in a laboratory fluidized bed, Fuel 245 (2019) 305-315. https://doi.org/10.1016/j.fuel.2019.02.034.
[36] Y. Zhao, G. Liu, J. Huang, A. Veksha, X. Wu, A. Giannis, T.T. Lim, G. Lisak, Sorbents for high-temperature removal of alkali metals and HCl from municipal solid waste derived syngas, Fuel 321 (2022). https://doi.org/10.1016/j.fuel.2022.124058.
[37] J. Cao, W. Zhong, B. Jin, Z. Wang, K. Wang, Treatment of Hydrochloric Acid in Flue Gas from Municipal Solid Waste Incineration with Ca–Mg–Al Mixed Oxides at Medium–High Temperatures, Energy & Fuels 28(6) (2014) 4112-4117. https://doi.org/10.1021/ef5008193.
[38] E.R. Monazam, R. Siriwardane, Hydrogen Production by Steam Oxidation of Reduced CaFe2O4 during Chemical Looping Coal Gasification: Equilibrium and Kinetic Analysis, Energy & Fuels 32(10) (2018) 10398-10407. https://doi.org/10.1021/acs.energyfuels.8b01650.
[39] P. Cho, T. Mattisson, A. Lyngfelt, Defluidization Conditions for a Fluidized Bed of Iron Oxide-, Nickel Oxide-, and Manganese Oxide-Containing Oxygen Carriers for Chemical-Looping Combustion, Industrial & Engineering Chemistry Research 45 (2005) 968-977. https://doi.org/doi.org/10.1021/ie050484d.

[40] D.D. Miller, J. Riley, R. Siriwardane, Interaction of Methane with Calcium Ferrite in the Chemical Looping Partial Oxidation Application: Experimental and DFT Study, Energy & Fuels 34(2) (2019) 2193-2204. https://doi.org/10.1021/acs.energyfuels.9b03623.
[41] R.A. Barros do Nascimento, H. Pimenta de Macedo, D.M.A. Melo, R.C. Santiago, T. Rodrigues de Araújo, R.L.B.A. Medeiros, J. Adánez, Structure and Reactivity of Brazilian Iron Ores as Low-Cost Oxygen Carriers for Chemical Looping Combustion, Industrial & Engineering Chemistry Research 61(6) (2022) 2469-2482. https://doi.org/10.1021/acs.iecr.1c03763.
[42] N. Husnain, E. Wang, S. Fareed, M. Tuoqeer Anwar, Comparision on the Low-Temperature NH3-SCR Performance of γ-Fe2O3 Catalysts Prepared by Two Different Methods, Catalysts 9(12) (2019). https://doi.org/10.3390/catal9121018.
[43] C. Liu, J. Luo, H. Dong, Z. Zhao, C. Xu, S. Abuelgasim, A. Abdalazeez, W. Wang, D. Chen, Q. Tang, Hydrogen-rich syngas production form biomass char by chemical looping gasification with Fe/Ca-based oxygen carrier, Separation and Purification Technology 300 (2022). https://doi.org/10.1016/j.seppur.2022.121912.
[44] J. Luan, R. Li, Z. Zhang, Y. Li, Y. Zhao, Influence of chlorine, sulfur and phosphorus on the volatilization behavior of heavy metals during sewage sludge thermal treatment, Waste Manag Res 31(10) (2013) 1012-8. https://doi.org/10.1177/0734242X13493955.
[45] B. Galey, M. Gautier, B. Kim, D. Blanc, V. Chatain, G. Ducom, N. Dumont, R. Gourdon, Trace metal elements vaporization and phosphorus recovery during sewage sludge thermochemical treatment - A review, J Hazard Mater 424(Pt B) (2022) 127360. https://doi.org/10.1016/j.jhazmat.2021.127360.
[46] S. Wang, L. Zhou, M. Zheng, J. Han, R. Liu, J. Yun, Catalytic Ozonation over Ca2Fe2O5 for the Degradation of Quinoline in an Aqueous Solution, Industrial & Engineering Chemistry Research 61(19) (2022) 6343-6353. https://doi.org/10.1021/acs.iecr.2c00464.
[47] X. Sun, W. Xiang, S. Wang, W. Tian, X. Xu, Y. Xu, Y. Xiao, Investigation of coal fueled chemical looping combustion using Fe3O4 as oxygen carrier: Influence of variables, Journal of Thermal Science 19(3) (2010) 266-275. https://doi.org/10.1007/s11630-010-0266-3.
[48] Z. Miao, E. Jiang, Z. Hu, Review of agglomeration in biomass chemical looping technology, Fuel 309 (2022). https://doi.org/10.1016/j.fuel.2021.122199.
[49] W. Liu, M. Ismail, M.T. Dunstan, W. Hu, Z. Zhang, P.S. Fennell, S.A. Scott, J.S. Dennis, Inhibiting the interaction between FeO and Al2O3 during chemical looping production of hydrogen, RSC Advances 5(3) (2015) 1759-1771. https://doi.org/10.1039/c4ra11891j.
[50] Q. Zafar, T. Mattisson, B. Gevert, Redox investigation of some oxides of transition-state metals Ni, Cu, Fe and Mn supported on SiO2 and MgAl2O4, Energy & Fuels 20 (2006) 34-44. https://doi.org/https://doi.org/10.1021/ef0501389.
[51] Y. Gan, H.M. El-Houjeiri, A. Badahdah, Z. Lu, H. Cai, S. Przesmitzki, M. Wang, Carbon footprint of global natural gas supplies to China, Nat Commun 11(1) (2020) 824. https://doi.org/10.1038/s41467-020-14606-4.
[52] R.K. Pachauri, M.R. Allen, V.R. Barros, J. Broome, W. Cramer, R. Christ, J.A. Church, L. Clarke, D. Qin, P. Dasgupta, N.K. Dubash, O. Edenhofer, I. Elgizouli, C.B. Field, P. Forster, P. Friedlingstein, J. Fuglestvedt, L. Gomez-Echeverri, S. Hallegatte, G. Hegerl, M. Howden, K. Jiang, B.J. Cisneros, V. Kattsov, H. Lee, K.J. Mach, J. Marotzke, M.D. Mastrandrea, L. Meyer, J. Minx, Y. Mulugetta, K. O'Brien, M. Oppenheimer, J.J. Pereira, R. Pichs-Madruga, G.K. Plattner, H.O. Pörtner, S.B. Power, B. Preston, N.H. Ravindranath, A. Reisinger, K. Riahi, M. Rusticucci, R. Scholes, K. Seyboth, Y. Sokona, R. Stavins, T.F. Stocker, P. Tschakert, D. van Vuuren, J.P. van Ypersele, IPCC Fifth Assessment Synthesis Report-Climate Change 2014 Synthesis Report, Intergovernmental Panel on Climate Change, Geneva, Switzerland, 2014, pp. 76-88.
[53] B. Hmiel, V.V. Petrenko, M.N. Dyonisius, C. Buizert, A.M. Smith, P.F. Place, C. Harth, R. Beaudette, Q. Hua, B. Yang, I. Vimont, S.E. Michel, J.P. Severinghaus, D. Etheridge, T. Bromley, J. Schmitt, X. Fain, R.F. Weiss, E. Dlugokencky, Preindustrial (14)CH(4) indicates greater anthropogenic fossil CH(4) emissions, Nature 578(7795) (2020) 409-412. https://doi.org/10.1038/s41586-020-1991-8.
[54] The Observatory of Economic Complexity, Where does Singapore import Iron Ore from? (2020), 2020. https://oec.world/en/visualize/tree_map/hs92/import/sgp/show/52601/2020/. (Accessed 27 January 2023 2023).
[55] M. Yellishetty, P.G. Ranjith, A. Tharumarajah, Iron ore and steel production trends and material flows in the world: Is this really sustainable?, Resources, Conservation and Recycling 54(12) (2010) 1084-1094. https://doi.org/10.1016/j.resconrec.2010.03.003.
[56] R. Cossu, I.D. Williams, Urban mining: Concepts, terminology, challenges, Waste Manag 45 (2015) 1-3. https://doi.org/10.1016/j.wasman.2015.09.040.
[57] J. Dai, L. Hughey, K.J. Whitty, Influence of fuel ash on the recoverability of copper from the spent material of chemical looping combustion, Fuel Processing Technology 201 (2020).

https://doi.org/10.1016/j.fuproc.2020.106358.
[58] R. Singh, Introduction, Applied Welding Engineering2016, pp. 3-5. https://doi.org/10.1016/b978-0-12-804176-5.00001-3.
[59] T. Ahmad, K. Ahmad, M. Alam, Sustainable management of water treatment sludge through 3'R' concept, Journal of Cleaner Production 124 (2016) 1-13. https://doi.org/10.1016/j.jclepro.2016.02.073.
[60] M. Qasim, M. Ayoub, N.A. Ghazali, A. Aqsha, M. Ameen, Recent Advances and Development of Various Oxygen Carriers for the Chemical Looping Combustion Process: A Review, Industrial & Engineering Chemistry Research 60(24) (2021) 8621-8641. https://doi.org/10.1021/acs.iecr.1c01111.
[61] S.L. Ng, L.M. Chu, S.H. Chan, A.T.H. Ma, The potential use of waterworks sludge in greening: A bioassay with bermudagrass [Cynodon dactylon (L.) Pers.], Urban Forestry & Urban Greening 55 (2020). https://doi.org/10.1016/j.ufug.2020.126856.